Generation of narrowband pulses from chirped broadband pulse frequency mixing

Generation of narrowband pulses from chirped broadband pulse frequency mixing

TREVOR L. COURTNEY,[1] NILS TORGE MECKER,[2] BRIAN D. PATTERSON,[1] MARK LINNE,[2] AND CHRISTOPHER J. KLIEWER[1,*]

[1]*Combustion Research Facility, Sandia National Laboratories, Livermore, California 94551, USA*
[2]*School of Engineering, The University of Edinburgh, EH8 3JL Edinburgh, United Kingdom*
**Corresponding author: cjkliew@sandia.gov*

Received XX Month XXXX; revised XX Month, XXXX; accepted XX Month XXXX; posted XX Month XXXX (Doc. ID XXXXX); published XX Month XXXX

We extend an approach based upon sum-frequency generation of oppositely chirped pulses to narrow the bandwidths of broadband femtosecond pulses. We efficiently generate near transform-limited pulses with durations of several picoseconds while reducing the pulse bandwidth by a factor of 120, which is more than twice the reduction reported in previous literature. Such extreme bandwidth narrowing of a broadband pulse enhances the effects of dispersion nonlinearities. Precise chirp control enables us to characterize the efficacy of frequency mixing broadband pulses with nonlinear temporal chirps. We demonstrate the use of these narrowband pulses as probes in coherent anti-Stokes Raman spectroscopy.

OCIS codes: (320.1590) Chirping; (320.7110) Ultrafast nonlinear optics; (300.6230) Spectroscopy, coherent anti-Stokes Raman scattering

http://dx.doi.org/10.1364/OL.99.099999

Femtosecond laser systems are widely used in applications that require optical pulses of various repetition rates, pulse energies, and frequencies of light. Specifically, many spectroscopies require the time resolution and bandwidth of femtosecond transform-limited (TL) pulses. Other spectroscopies rely on the frequency resolution of narrowband, picosecond TL pulses. Femtosecond and picosecond pulses combine in femtosecond stimulated Raman spectroscopy (FSRS)[1-2] and in certain coherent anti-Stokes Raman spectroscopy (CARS)[3-5] and sum frequency generation (SFG) spectroscopy [6-7] experiments. All of these experiments benefit from bandwidth-narrowing methods that enable the use of a single laser system. Grating filtering and frequency doubling in thick nonlinear crystals suffer from inefficiency and damage threshold power limits. Alternatively, nonlinear frequency mixing of chirped pulses is an efficient method initially demonstrated using SFG of oppositely chirped pulses [8]. This bandwidth reduction concept has been adapted to mid-infrared and terahertz radiation by difference frequency mixing (DFG) equally chirped pulses [9-14] and extended by pumping a noncollinear optical parametric amplifier (NOPA) with narrowed SFG pulses for tunable near-ultraviolet through near-infrared pulses in FSRS [15-17]. Researchers have also used chirped pulse SFG for high energy pulses in gas-phase CARS experiments [18-20].

Chirped pulse mixing designs reported over the last two decades typically begin with compressed laser system outputs. For chirped pulse SFG, also termed second-harmonic bandwidth compression (SHBC), one output is split into two beams of TL pulse replicas, which are then oppositely chirped. The linearly chirped pulses overlap spatially and temporally in a nonlinear crystal such that all time-coincident frequency pairs have nearly the same phase-matching requirements and frequency sums. A positive (negative) chirp is typically provided by a grating stretcher (compressor), often half of a 4*f* design stretcher [18]. This simplification is chosen for compact and economical design [17, 19]; it reduces losses at the expense of creating slight spatial chirp on the fundamental beam [10]. However, initial compression to TL pulses causes unnecessary power losses.

In this Letter, we present a bandwidth-narrowing method based on the original design of Raoult, et al., [8] which involves adjusting the chirp of uncompressed amplified laser pulses. Here, we characterize the broadband chirped SFG process and introduce optical system modifications for this regime. We use a Coherent Legend Elite Ti:Sapphire regenerative amplifier (795 nm, 1 kHz) seeded by a Coherent Vitara oscillator (100 MHz). The amplified beam is split into two beams; each beam is single-pass amplified to ~9 mJ/pulse. One temporally stretched (>100 ps, positively chirped) output is used for chirped pulse SFG (Fig. 1a). This beam is evenly split between two grating compressors, each with two gratings (Spectrogon, 1500 grooves/mm) separated by $L\pm\delta$, where $L \approx 305$ mm is the distance required for 40 fs TL pulse compression. For positive δ, a separation of $L-\delta$ leaves a slight residual positive chirp; an equal magnitude negative chirp results from $L+\delta$ (Fig. 1a). Each compressor maintains >80% throughput after four grating reflections that eliminate spatial chirp in the fundamental beams. A large δ (≈28 mm) enables fine control of δ for precise chirp matching, which can be more difficult to achieve in the minimally

chirped pulses of other designs [19]. A translation stage in the L+δ path controls the delay, τ, between compressor arms and tunes the SFG spectrum. The fundamental beams have a small (1°) crossing angle in a 1 mm BBO crystal (Type I) to minimize spatial chirp in the SFG pulses while enabling spatial isolation of the desired beam. From the combined 6 mJ/pulse of fundamental beams, the conversion efficiency is 20-30%, depending on δ and SFG bandwidth. Pulses centered at $\lambda_{SFG} \approx 396.3$ nm with $\Delta\nu_{SFG} = 3.0$ cm^{-1} full width at half maximum (FWHM) bandwidth and FWHM duration of $\Delta t = 5.5$ ps have 1.2 mJ/pulse (20% efficiency).

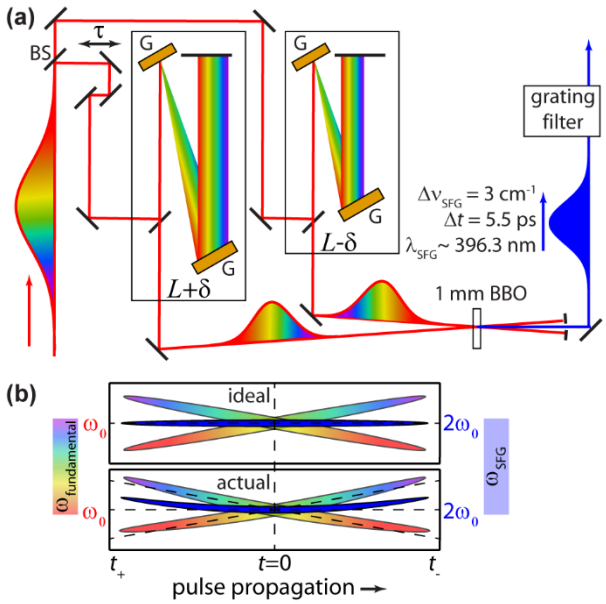

Fig. 1. Chirped pulse sum frequency generation. (a) The amplified, positively chirped (>100 ps) Ti:Sapphire output is split between two grating compressors. The pulses in the L-δ path remain slightly positively chirped; the other path pulses are delayed by τ and become negatively chirped (L+δ). Narrowband pulses are generated in BBO. (b) Cartoon: oppositely chirped fundamental pulses and upconverted pulse in time for ideal linear temporal chirp with respect to frequency (top panel) and temporal chirp with nonlinearities (bottom panel).

SHBC pulses from femtosecond lasers have had bandwidths reduced to as low as $\Delta\nu_{SFG} \approx 3.5$ cm^{-1} [8, 18]. However, the fundamental bandwidths vary among the laser systems used in SHBC, so the reduction factor $\Delta\nu_R = \Delta\nu_{fundamental} / \Delta\nu_{SFG}$ quantifies the process. Calculated or inferred $\Delta\nu_R$ literature values are ~20-40 for ≥100 fs systems [8, 18] and ~60 in broadband laser systems narrowed to $\Delta\nu \geq 7.0$ cm^{-1} [17, 19]. In this work, we narrow a broadband pulse to achieve $\Delta\nu_R = 360\ \text{cm}^{-1} / 3\ \text{cm}^{-1} = 120$. A broadband fundamental pulse is beneficial in two-beam fs/ps pure-rotational CARS (RCARS) [5], for example, to excite coherences of large Raman shifts without bandwidth broadening via multiple pulses [18, 21]. In reducing this bandwidth significantly, we magnify the sensitivity of the chirped pulse SFG process to a key experimental approximation: frequency linearity of temporal chirp. The process shown in the top panel of Fig. 1b can be written as a time-independent SFG frequency, ω_3, of oppositely chirped pulses, $\omega_1(t) = \omega_0 + at$ and $\omega_2(t) = \omega_0 - a(t-\tau)$ with delay, τ, center frequency, ω_0, and linear temporal chirp, $a = d\omega / dt$:

$$\omega_3 = 2\omega_0 + a\tau, \qquad (1)$$

where ω_3 can be tuned by changing τ [8]. Nearly all SHBC stretcher and compressor designs have used gratings, which diffract light nearly linearly with wavelength, as given by the grating equation. The specific gratings and angles used determine the change in compressor round trip delay over the pulse spectrum, which can be described by a or by the second-order phase, $d^2\phi / dt^2$. Researchers have also chirped via prism compressors and material dispersion in SFG [22] and DFG techniques [11-13]. Prism compressors, bulk materials, and grating compressors, in general, have higher-order phase contributions, i.e., a and $d^2\phi / dt^2$ are not constant in ω. To find the group delay in our system, we invert a to obtain the group delay dispersion (GDD) and integrate, as in $\int d\omega / a(\omega)$. For each compressor, the relative group delay can be calculated with respect to the delay of ω_0. The optical path delay between compressor outputs is set such that $\tau = 0$ defines the temporal overlap between each ω_0. With nonlinear temporal chirp, all other time-coincident interpulse frequency pairs (ω_1, ω_2) are asymmetric about ω_0 and result in a time-dependent $\omega_3(t)$ that is blue-shifted from its minimum ($2\omega_0$) at early and late t (t_- and t_+ in Fig. 1b, bottom panel). Concomitantly, other ω_1, ω_2 pairs that would sum to $\omega_3 = 2\omega_0$ do not produce SFG, as they have increasingly nonzero delays with displacement from ω_0.

To illustrate the effects of the nonlinear chirp, we upconvert oppositely chirped pulses for six cases of δ, maintaining $\tau \approx 0$ and $\omega_3(0)$. The SFG spectra are displayed in Fig. 2a for δ, given as the percent δ/L, increasing top to bottom: 3.4, 4.9, 6.3, 7.8, 9.2, and 10.6 %. Increasing the temporal chirp generates pulses with narrower spectra, centered at $\nu_c \approx 25235$ cm^{-1}. In the limit of spectrally constant GDD or a, this effect arises from the increased isolation of complementary ω_1, ω_2 pairs to narrow ω_3. Unchirped SFG pulses have bandwidths dictated by the temporal durations of the chirped pulses. The higher-order nonlinear phases of fundamental pulses limit the minimum SFG bandwidth, and increasing the fundamental chirp beyond this limit results in chirped SFG pulses (evident in large time-bandwidth products in Ref. [8]). As shown in Fig. 2a, the spectrum for each δ follows a Gaussian shape at low frequencies but displays a high-frequency spectral wing (Fig. 2a). Oscillations in this wing arise from the interferences between light at ω_3 in the t_- and t_+ portions of the pulse. Setting $\tau = 0$ for simplicity, symmetric time points about $t = 0$ with ω_3-dependent delay, $\Delta t_\omega = t_+ - t_-$, produce frequency-matched pairs of SFG intensities, $I^+(\omega_3)$ and $I^-(\omega_3)$. For each $\Delta t_\omega \neq 0$, the corresponding ω_3 is produced at temporally isolated points on either side of $t = 0$.

Integrated over t, the detected spectral intensity is given by,

$$I(\omega_3) = I^+(\omega_3) + I^-(\omega_3) + 2E^+(\omega_3)E^-(\omega_3)\cos(\omega_3 \Delta t_\omega). \qquad (2)$$

The non-oscillatory component, $I^+(\omega_3)+I^-(\omega_3)$, is modeled for the largest δ in Fig. 2a (dashed line). The blue-shift from ν_c of the half-maximum intensity in this trace corresponds to the blue-shift of ω_3 when considering the ω_1, ω_2 pairs that have matched group delays and frequencies separated by the fundamental pulse spectrum FWHM. We perform a Fourier transform (FT) on each trace after subtracting its non-oscillatory component, which results in broad features as Δt_ω evolves with ω_3 (Fig. 2b). The largest peaks are centered near the measured δ-dependent chirped fundamental pulse FWHM temporal durations, e.g., ~10.5 ps peak (red trace) for δ = 28 mm. For our grating compressors, the delay between the ω_1, ω_2 pair that spans the fundamental FWHM bandwidth at t_- and the one at t_+ is calculated for each of the six δ values: 3.9, 5.5, 7.1, 8.8, 10.4, and 12.0 ps for increasing δ. These delays roughly match the positions of the broad peaks in Fig. 2b; thus, the oscillations in Fig. 2a are dominated by ω_1, ω_2 pairs near the spectral FWHM. Contributions from ω_1, ω_2 pairs located closer to ω_0 are evident in smaller Δt_ω features in the FT (Fig. 2a) and from the asymmetry of the ν_c peak (Fig. 2b).

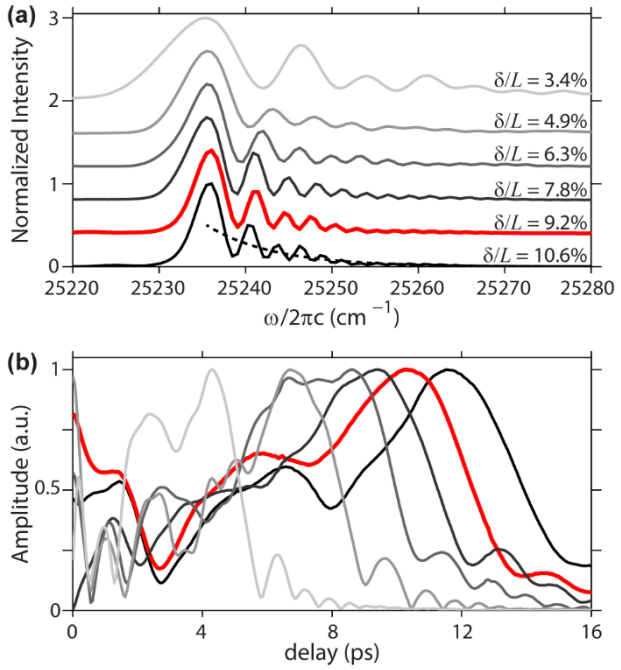

Fig. 2. Spectral analysis. (a) Narrowband spectra, offset for clarity, of 6 fundamental pulse chirp cases. The spectral widths of the dominant $\nu_c \approx$ 25235 cm^{-1} peaks decrease as δ increases, top to bottom. Oscillations exist at blue-shifted upconverted frequencies; example non-oscillatory component is shown (black dashed line). (b) The FT of the spectra in (a) display broad features at time separations between matched SFG frequencies. (a,b) Default chirp conditions in this work (red traces).

We exploit the SFG oscillations for precise chirp matching. The SFG of pulses with unmatched temporal chirps produces a spectrum with diminished and irregular oscillations, increased low-frequency intensity, and broadening of the central peak. For δ = 28 mm (Fig. 2, red traces), we match the magnitude of the dispersion between the two compressors to within Δδ = 0.5 mm (~1.6% of δ). The L+δ compressor separation is stepped by 0.44 mm, while τ is adjusted to maintain ν_c. The vertical axis of Fig. 3a is centered on the initial determination of matched temporal chirps ($\Delta\delta_{initial} = 0$) based on narrowest spectrum and maximum SFG intensity. Each horizontal white line in Fig. 3a denotes a spectral slice shown in the same vertical order in Fig. 3c. The thickest line in each figure corresponds to the most accurately determined Δδ = 0, which produces the greatest fringe depth in blue SFG interferences.

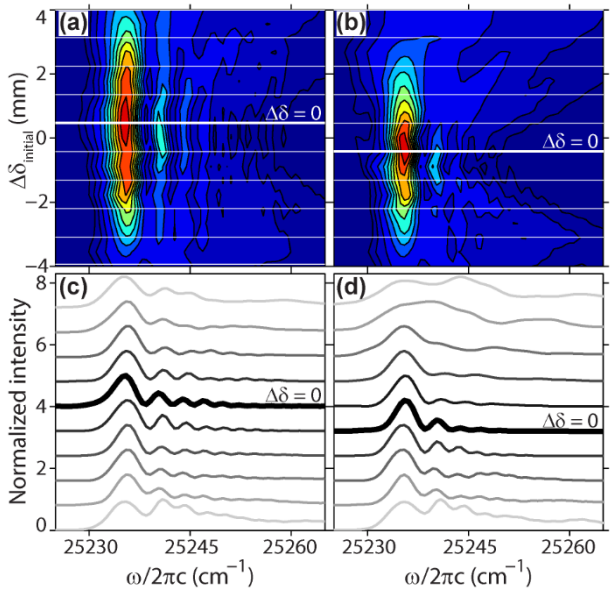

Fig. 3. Opposite chirp matching without (a) and with (b) a short-pass filter in the positively chirped pulse. (a, b) SHBC spectra for a series of grating separations in the negative chirp compressor. (c, d) Spectral slices from $\Delta\delta_{initial}$ marked with white lines in (a, b), in same vertical order. Traces normalized and offset for clarity. Bold trace indicates ideal grating separation (Δδ = 0).

The removal of the blue wing in the SFG spectrum is essential for simplifying the lineshapes of narrow spectroscopic transitions, such as those in nitrogen (N_2) gas-phase RCARS (Fig. 4). We first consider indirectly shaping the SFG spectrum by addressing the fundamental pulse nonlinear chirp. Conceivably, the higher-order phase terms of the compressor could be offset by material dispersion. Given the significant higher-order dispersion in this grating-based design, we choose the simpler method of reducing the fundamental bandwidth. Careful spectral filtering of the fundamental pulses enables SFG of a bandwidth over which the temporal chirp can be approximated as linear in frequency. Without a Fourier plane compressor, we insert an angle-tuned short-pass filter (FF01-842/SP-25 Semrock) in the L-δ compressor output and adjust τ to preserve ν_c (Fig. 3b, spectral slices in Fig. 3d). The top few spectra in Figs. 3b,d exhibit weak SFG, as more spectral intensity in the overly negatively chirped pulses has no temporal match. As expected, the true Δδ = 0 vertical position is slightly shifted (bold lines, Figs. 3b,d) compared to Figs. 3a,c to give the narrowest SFG spectrum from a reduced fundamental bandwidth with shifted spectral center. We choose to filter out a fundamental pulse leading edge (lower right quadrant of Fig. 1b, bottom panel) so the SFG pulse has a steep, clean early time profile, which is ideal for its use as a spectroscopic probe at minimal delays from a pump pulse. The resulting SFG spectra are

narrower, with steeper low-frequency decays and high-frequency wings reduced from Eq. (2) to $I(\omega_3) = I^+(\omega_3)$ where fundamental frequencies are extinguished. Oscillatory features persist closer to ν_c but can be reduced beyond those in Fig. 3d by stacking two spectral filters, further suppressing the wing without broadening the SFG by excessive filtering in either pulse of spectral content in the lower quadrants in Fig. 1b, bottom panel. A portion of the resulting SFG beam is used to probe the N_2 RCARS coherence induced by a 40 fs Ti:Sapphire pump/Stokes pulse. The high-frequency probe shoulder is evident in the blue wings of rotational lines in the spectrum (Fig. 4a, gray trace), an artifact that is less important for systems with broader spectral features or more widely spaced transitions.

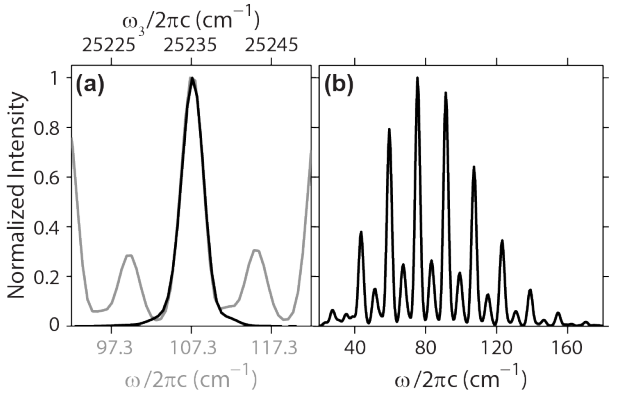

Fig. 4. Narrowband probe and fs/ps RCARS spectra. (a) N_2 RCARS spectrum (gray trace, lower gray x-axis) taken with probe after fundamental spectral filtering but before SFG grating filtering. Grating filtered $\Delta\nu$ = 3.0 cm^{-1} probe spectrum (black trace, upper black x-axis). (b) Spectrum of 7.8 atm of N_2 at room temperature, probed at 8 ps delay (transitions out of rotational states J = [2, 20]) by probe from (a).

To achieve ideal gas-phase RCARS lineshapes, the 1.2 mJ SFG pulses (δ = 28 mm, spectrally filtered) are sent through a folded 4f grating filter (f = 1 m, 1800 grooves/mm) to remove remaining spectral wings without reducing $\Delta\nu$. Compared to the bandwidth narrowing of broadband pulses solely by grating filtering the fundamental, this spectral refinement strategy suffers from less intensity loss, which is primarily dictated by grating efficiency. For very large δ (Fig. 2a, bottom trace), the close-lying interference peak cannot be separated from the ν_c peak. The final probe (Fig. 4a, black trace) is used to generate the N_2 RCARS spectrum in Fig. 4b, which has closely spaced (8 cm^{-1} separation) but frequency resolved transitions for straightforward modeling. Therefore, this is an effective method to produce a narrowband probe with high resolving power from a broadband laser capable of impulsive excitation of Raman coherences beyond 500 cm^{-1}. Bandwidth narrowing of 100-fs duration laser pulses in this manner would be simpler, since the grating-pair produced chirp over the correspondingly smaller fundamental spectral range could be more closely approximated as linear in frequency.

In summary, we have reported the largest bandwidth reduction to date using the efficient technique of spectral narrowing via oppositely chirped pulse SFG. Furthermore, we have investigated the consequences of nonlinear chirp in broadband pulses and presented a combination of filtering techniques to overcome this limitation. The method presented in this Letter provides a versatile laser system of high energy pulses of significantly different bandwidths, with which we perform RCARS measurements of gas-phase N_2 to demonstrate one of many potential applications.

Funding. National Nuclear Security Administration (NNSA) (DE-NA0003525); Sandia National Laboratories.

Acknowledgment. The equipment for this work was supported by the Division of Chemical Sciences, Geosciences, and Biosciences, the Office of Basic Energy Sciences (BES), the U.S. Department of Energy (DOE) under the Early Career Research Program (CJK). TLC, CJK, experiment construction, and grating compressors were supported by the Laboratory Directed Research and Development (LDRD) program at Sandia National Laboratories, which is a multimission laboratory managed and operated by National Technology and Engineering Solutions of Sandia, LLC., a wholly owned subsidiary of Honeywell International, Inc., for the U.S. Department of Energy's National Nuclear Security Administration under Contract DE-NA0003525. The views expressed in the article do not necessarily represent the views of the U.S. Department of Energy or the United States Government.

References

1. D. W. McCamant, P. Kukura, and R. A. Mathies, J. Phys. Chem. A **107**, 8208 (2003).
2. D. W. McCamant, P. Kukura, S. Yoon, and R. A. Mathies, Rev. Sci. Instrum. **75**, 4971 (2004).
3. B. D. Prince, A. Chakraborty, B. M. Prince, and H. U. Stauffer, J. Chem. Phys. **125**, 044502 (2006).
4. J. D. Miller, S. Roy, M. N. Slipchenko, J. R. Gord, and T. R. Meyer, Opt. Express **19**, 15627 (2011).
5. A. Bohlin, B. D. Patterson, and C. J. Kliewer, J. Chem. Phys. **138**, 081102 (2013).
6. L. J. Richter, T. P. Petralli-Mallow, and J. C. Stephenson, Opt. Lett. **23**, 1594 (1998).
7. I. V. Stiopkin, H. D. Jayathilake, A. N. Bordenyuk, and A. V. Benderskii, J. Am. Chem. Soc. **130**, 2271 (2008).
8. F. Raoult, A. C. L. Boscheron, D. Husson, C. Sauteret, A. Modena, V. Malka, F. Dorchies, and A. Migus, Opt. Lett. **23**, 1117 (1998).
9. G. Veitas, and R. Danielius, J. Opt. Soc. Am. B **16**, 1561 (1999).
10. G. Veitas, R. Danielius, and E. Schreiber, J. Opt. Soc. Am. B **19**, 1411 (2002).
11. F. O. Koller, K. Haiser, M. Huber, T. E. Schrader, N. Regner, W. J. Schreier, and W. Zinth, Opt. Lett. **32**, 3339 (2007).
12. S. Wandel, M. W. Lin, Y. C. Yin, G. B. Xu, and I. Jovanovic, J. Opt. Soc. Am. B **33**, 1580 (2016).
13. A. Cartella, T. F. Nova, A. Oriana, G. Cerullo, M. Forst, C. Manzoni, and A. Cavalleri, Opt. Lett. **42**, 663 (2017).
14. A. S. Weling, B. B. Hu, N. M. Froberg, and D. H. Auston, Appl. Phys. Lett. **64**, 137 (1994).
15. S. Laimgruber, H. Schachenmayr, B. Schmidt, W. Zinth, and P. Gilch, Appl. Phys. B **85**, 557 (2006).
16. S. A. Kovalenko, A. L. Dobryakov, and N. P. Ernsting, Rev. Sci. Instrum. **82**, 063102 (2011).
17. L. D. Zhu, W. M. Liu, and C. Fang, Appl. Phys. Lett. **105**, (2014).
18. S. P. Kearney, and D. J. Scoglietti, Opt. Lett. **38**, 833 (2013).
19. C. B. Yang, D. Escofet-Martin, D. Dunn-Rankin, Y. C. Chien, X. Yu, and S. Mukamel, J. Raman Spectrosc. **48**, 1881 (2017).
20. S. P. Kearney, Combust. Flame **162**, 1748 (2015).
21. S. P. Kearney, Appl. Optics **53**, 6579 (2014).
22. K. Osvay, and I. N. Ross, Opt. Commun. **166**, 113 (1999).

Full References

1. D. W. McCamant, P. Kukura, and R. A. Mathies, Femtosecond Time-Resolved Stimulated Raman Spectroscopy: Application to the Ultrafast Internal Conversion in Beta-Carotene, J. Phys. Chem. A **107**, 8208-8214 (2003).
2. D. W. McCamant, P. Kukura, S. Yoon, and R. A. Mathies, Femtosecond Broadband Stimulated Raman Spectroscopy: Apparatus and Methods, Rev. Sci. Instrum. **75**, 4971-4980 (2004).
3. B. D. Prince, A. Chakraborty, B. M. Prince, and H. U. Stauffer, Development of Simultaneous Frequency- and Time-Resolved Coherent Anti-Stokes Raman Scattering for Ultrafast Detection of Molecular Raman Spectra, J. Chem. Phys. **125**, 044502 (2006).
4. J. D. Miller, S. Roy, M. N. Slipchenko, J. R. Gord, and T. R. Meyer, Single-Shot Gas-Phase Thermometry Using Pure-Rotational Hybrid Femtosecond/Picosecond Coherent Anti-Stokes Raman Scattering, Opt. Express **19**, 15627-15640 (2011).
5. A. Bohlin, B. D. Patterson, and C. J. Kliewer, Communication: Simplified Two-Beam Rotational CARS Signal Generation Demonstrated in 1D, J. Chem. Phys. **138**, 081102 (2013).
6. L. J. Richter, T. P. Petralli-Mallow, and J. C. Stephenson, Vibrationally Resolved Sum-Frequency Generation with Broad-Bandwidth Infrared Pulses, Opt. Lett. **23**, 1594-1596 (1998).
7. I. V. Stiopkin, H. D. Jayathilake, A. N. Bordenyuk, and A. V. Benderskii, Heterodyne-Detected Vibrational Sum Frequency Generation Spectroscopy, J. Am. Chem. Soc. **130**, 2271-2275 (2008).
8. F. Raoult, A. C. L. Boscheron, D. Husson, C. Sauteret, A. Modena, V. Malka, F. Dorchies, and A. Migus, Efficient Generation of Narrow-Bandwidth Picosecond Pulses by Frequency Doubling of Femtosecond Chirped Pulses, Opt. Lett. **23**, 1117-1119 (1998).
9. G. Veitas and R. Danielius, Generation of Narrow-Bandwidth Tunable Picosecond Pulses by Difference-Frequency Mixing of Stretched Pulses, J. Opt. Soc. Am. B **16**, 1561-1565 (1999).
10. G. Veitas, R. Danielius, and E. Schreiber, Efficient Generation of < 3-cm-1 Bandwidth Mid-IR Pulses by Difference-Frequency Mixing of Chirped Pulses, J. Opt. Soc. Am. B **19**, 1411-1418 (2002).
11. F. O. Koller, K. Haiser, M. Huber, T. E. Schrader, N. Regner, W. J. Schreier, and W. Zinth, Generation of Narrowband Subpicosecond Mid-Infrared Pulses Via Difference Frequency Mixing of Chirped Near-Infrared Pulses, Opt. Lett. **32**, 3339-3341 (2007).
12. S. Wandel, M. W. Lin, Y. C. Yin, G. B. Xu, and I. Jovanovic, Bandwidth Control in 5 μm Pulse Generation by Dual-Chirped Optical Parametric Amplification, J. Opt. Soc. Am. B **33**, 1580-1587 (2016).
13. A. Cartella, T. F. Nova, A. Oriana, G. Cerullo, M. Forst, C. Manzoni, and A. Cavalleri, Narrowband Carrier-Envelope Phase Stable Mid-Infrared Pulses at Wavelengths Beyond 10 μm by Chirped-Pulse Difference Frequency Generation, Opt. Lett. **42**, 663-666 (2017).
14. A. S. Weling, B. B. Hu, N. M. Froberg, and D. H. Auston, Generation of Tunable Narrow-band THz Radiation from Large-Aperture Photoconducting Antennas, Appl. Phys. Lett. **64**, 137-139 (1994).
15. S. Laimgruber, H. Schachenmayr, B. Schmidt, W. Zinth, and P. Gilch, A Femtosecond Stimulated Raman Spectrograph for the Near Ultraviolet, Appl. Phys. B **85**, 557-564 (2006).
16. S. A. Kovalenko, A. L. Dobryakov, and N. P. Ernsting, An Efficient Setup for Femtosecond Stimulated Raman Spectroscopy, Rev. Sci. Instrum. **82**, 063102 (2011).
17. L. D. Zhu, W. M. Liu, and C. Fang, A Versatile Femtosecond Stimulated Raman Spectroscopy Setup with Tunable Pulses in the Visible to Near Infrared, Appl. Phys. Lett. **105**, (2014).
18. S. P. Kearney and D. J. Scoglietti, Hybrid Femtosecond/Picosecond Rotational Coherent Anti-Stokes Raman Scattering at Flame Temperatures Using a Second-Harmonic Bandwidth-Compressed Probe, Opt. Lett. **38**, 833-835 (2013).
19. C. B. Yang, D. Escofet-Martin, D. Dunn-Rankin, Y. C. Chien, X. Yu, and S. Mukamel, Hybrid Femtosecond/Picosecond Pure-Rotational Coherent Anti-Stokes Raman Scattering with Chirped Probe Pulses, J. Raman Spectrosc. **48**, 1881-1886 (2017).
20. S. P. Kearney, Hybrid fs/ps Rotational CARS Temperature and Oxygen Measurements in the Product Gases of Canonical Flat Flames, Combust. Flame **162**, 1748-1758 (2015).
21. S. P. Kearney, Bandwidth Optimization of Femtosecond Pure-Rotational Coherent Anti-Stokes Raman Scattering by Pump/Stokes Spectral Focusing, Appl. Optics **53**, 6579-6585 (2014).
22. K. Osvay and I. N. Ross, Efficient Tuneable Bandwidth Frequency Mixing Using Chirped Pulses, Opt. Commun. **166**, 113-119 (1999).